# Linear stability analysis on a spherical particle growing from a binary melt under the far-field flow*

Cao Bin(曹 斌), Lin Xin(林 鑫)†,
Wang Meng(王 猛), and Huang Wei-Dong(黄卫东)

*State Key Laboratory of Solidification Processing, Northwestern Polytechnical University, Xi'an* 710072, *China*

(Received 27 November 2011; revised manuscript received 28 December 2011)

The solutions of temperature and solute fields around a spherical crystal growing from a binary melt under the far-field flow are obtained. Based on the results, a linear stability analysis on the spherical interface growing from the binary melt under the far-field flow is performed. It is found that the constitutional supercooling effect ahead of the spherical crystal interface under the far-field flow is enhanced compared with that without the flow. The growth rate of the perturbation amplitude at the up-wind side of the spherical crystal interface is larger than that at the down-wind side. The critical stability radius of the crystal interface decreases with the increasing far-field flow velocity. Under the far-field flow, the whole spherical interface becomes more unstable compared with that without the flow.

**Keywords:** spherical crystal, far-field flow, interface stability, Trivedi's criterion

**PACS:** 64.70.D–, 64.70.dg, 81.10.Fq, 81.30.Fb **DOI:** 10.1088/1674-1056/21/5/056401

## 1. Introduction

The interaction between melt flow and solidification microstructure is one of the fundamental research fields in material science. To date, numerous studies have been focused on the relationships among interface stability, solute and heat transport, and liquid flow. Most of the research on the fluid flows' effects on the interface stability focused on the planar interface stability. Coriell *et al.*[1] studied the effect of a plane Couette flow on the interface stability. It was shown that for the interface perturbations with wavevectors parallel to the shear flow, the shear flow can stabilize the interface, while the shear flow does not affect the interface for the perturbations with wavevectors perpendicular to the flow. Brattkus and Davis[2] investigated the effect of the Stagnation-point flow on the planar interface stability. They found that the long wavelength disturbances can destabilize the interface. Davis and Schulze[3] later studied the stability of a system with oscillating solid in an elliptical orbit parallel to the interface. They concluded that an appropriate selection of the amplitude and the frequency of the modulation can eliminate the interface instability. Davis and Schulze[4] also showed that a proper selection of the parameters of the nonparallel shear flows can stabilize the planar interface during the directional solidification. Lin *et al.*[5] performed a linear stability analysis on a planar interface under the influence of fluid flow. They found that the fluid flow shortens the incubation time for the breakdown of the planar interface. Zhao and Li[6] employed the phase-field model to simulate the free dendritic growth process governed by the capillary anisotropy or the kinetic anisotropy. They discoverd that as the interface velocity increases, the cystal radius decreases. Sun *et al.*[7] developed a two-dimensional lattice Boltzmann method based model for the modelling of dendritic growth during the alloy solidification in the presence of forced and natural convections. It was found that the convection transports heat and solute from the upstream region to the downstream region, producing an asymmetrical dendrite that grows faster in the upstream direction but slower in the downstream direction. Xing *et al.*[8] showed that there is a linear relationship between the crystal growth velocity and the undercooling.

As for the spherical interface, Chen *et al.*[9] investigated the effect of far-field flow on the crystal growth

*Project supported by the National Natural Science Foundation of China (Grants Nos. 50771083 and 50901061), the National Basic Research Program of China (Grant No. 2011CB610402), the Fund of the State Key Laboratory of Solidification Processing in NWPU, China (Grants Nos. 02-TZ-2008 and 36-TP-2009), and the Programme of Introducing Talents of Discipline to Universities, China (Grant No. 08040).

†Corresponding author. E-mail: xlin@nwpu.edu.cn

© 2012 Chinese Physical Society and IOP Publishing Ltd

in the melt. It was shown that the moving velocity of the interface at the up-wind side is larger than that at the down-wind side. They also found that as the interface kinetic coefficient increases, the growth velocity of the spherical crystal increases.[10]

Several other studies[11−13] have considered the effect of the fluid flow, and most of them[11,13] are based on Trivedi's work. Trivedi[14] performed a linear stability analysis on the spherical interface growing from a binary melt without the flow and obtained a general marginal condition for the absolute shape stability

$$-G_{\mathrm{L}} + m_{\mathrm{L}} G_{\mathrm{C}} \xi(l) = \left(T_{\mathrm{M}} \Gamma / R_0^2\right) L, \tag{1}$$

where $m_{\mathrm{L}}$ is the slope of the liquidus, $G_{\mathrm{L}}$ is the temperature gradient, $G_{\mathrm{C}}$ is the solute gradient, $\Gamma$ is the Gibbs–Thompson parameter, $T_{\mathrm{M}}$ is the melting point, $R_0$ is the radius of the sphere, $l$ is the order of spherical harmonic, $\xi(l)$ and $L$ are both functions of $l$. Recently, we studied the effect of the shear flow on the stability of a spherical interface.[15] We found that the shear flow around the crystal can enhance the stability of the spherical interface. In another paper,[16] we used a perturbation series to obtain the solutions of the temperature and the solute fields.

In the present work, we investigate the influence of a far-field flow on the growth of a spherical crystal interface from a binary melt. First we study the effect of the far-field flow on the temperature and the solute fields around the crystal. To obtain the solutions of the temperature and the solute fields, we use the Laplace equation modified by the material derivatives. Then we perform a linear stability analysis of the spherical interface. We shall assume that the temperature and the solute fields change slowly with time so that we can ignore the time partial derivatives in the diffusion equations of heat flow and solute.[14]

This paper is divided into four parts. In Section 2, we obtain a solution for an unperturbed interface growing from a supercooled binary melt under the far-field flow and study the effect of the far-field flow on the temperature and the solute fields. In Section 3, we present a first order stability analysis of the spherical crystal interface. Then we calculate the growth rate of the perturbation amplitude and the critical radius below which the crystal interface is stable. In Section 4, we draw the conclusion.

## 2. Theoretical model

In the ground based solidification process, the fluid flow is unavoidable. Besides the natural convection, there are some forced flows driven by mechanical and electro-magnetical effects. In general, these fluid flows can be simplified as a far-field flow. Under the far-field flow, the crystal could present the translational motion and rotation. As for the crystal rotation, which will drive a shear flow around the crystal, we have already discussed its effect on the stability of the spherical crystal interface in a previous paper.[15] In the present work, we focus on the effect of the far-field flow on the stability of the static spherical interface, that is, the effect of the translational motion.

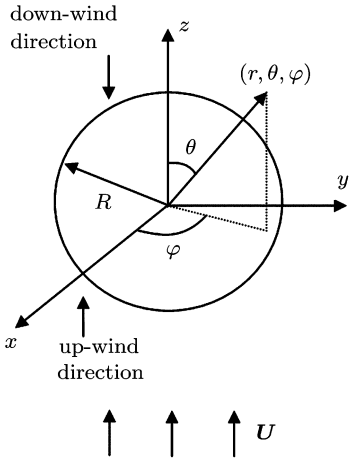



**Fig. 1.** Far field flow around a spherical crystal, where $\boldsymbol{U}$ represents the far-field velocity of the melt.

Consider a polar coordinate system with the $r$ axis located at the center of the crystal. Under the polar coordinates $(r, \theta, \varphi)$, we use $r = R(\theta, \varphi, t)$ to describe the spherical crystal interface growing from a supercooled binary melt, and $r = R_0(t)$ represents the unperturbed interface.

The heat and the solute fields will be governed by the following differential equations:

$$\boldsymbol{U} \cdot \boldsymbol{\nabla} T_{\mathrm{L}} = \left(k_{\mathrm{L}} / C_{\mathrm{pL}}\right) \Delta T_{\mathrm{L}}, \tag{2}$$

$$\Delta T_{\mathrm{S}} = 0, \tag{3}$$

$$\boldsymbol{U} \cdot \boldsymbol{\nabla} C = D \Delta C, \tag{4}$$

where $T_{\mathrm{L}}$ and $T_{\mathrm{S}}$ are the temperatures in the liquid and the solid, respectively, $C$ is the solute concentration of the liquid, $k_{\mathrm{L}}$ is the thermal conductivity of the liquid, $C_{\mathrm{pL}}$ is the specific heat per unit volume of the liquid, $D$ is the solute diffusion coefficient in the liquid, and $\boldsymbol{U}$ is the liquid-velocity vector.

The concentration at the interface is determined by the local temperature, which is given by the Gibbs–Thomson equation as

$$T_{\rm LI} = T_{\rm SI} = T_{\rm M} + m_{\rm L} C_{\rm I} - \Gamma T_{\rm M} K, \tag{5}$$

where subscript I denotes the value at the interface, $T_{\rm M}$ is the equilibrium melting temperature of the pure substance, $m_{\rm L}$ is the slope of the liquids, $\Gamma$ is the capillary constant, and $K$ is the curvature of the interface.

The interface velocity is determined by the heat and the mass conservation conditions at the interface

$$-h_\Delta \frac{\partial R}{\partial t} = k_{\rm L} \left(\frac{\partial T_{\rm L}}{\partial r}\right)_{\rm I} - k_{\rm S} \left(\frac{\partial T_{\rm S}}{\partial r}\right)_{\rm I}, \tag{6}$$

$$-C_{\rm I}\left(1-k_0\right)\frac{\partial R}{\partial t} = D\left(\frac{\partial C}{\partial r}\right)_{\rm I}, \tag{7}$$

where $\partial R/\partial t$ is the moving velocity of the interface, $h_\Delta$ is the latent heat of fusion per unit volume, and $k_0$ is the equilibrium solute distribution coefficient. We neglect the solute diffusion in the solid.

The expressions for flow field $\boldsymbol{U}$ around the spherical crystal under the far-field flow are[17]

$$U_R = U_\infty \cos\theta \left[1 - \frac{3}{2}\frac{R}{r} + \frac{1}{2}\left(\frac{R}{r}\right)^3\right], \tag{8}$$

$$U_\theta = -U_\infty \sin\theta \left[1 - \frac{3}{4}\frac{R}{r} - \frac{1}{4}\left(\frac{R}{r}\right)^3\right], \tag{9}$$

$$U_\varphi = 0, \tag{10}$$

where $U_R$ is the velocity in the $r$ direction, $U_\theta$ is the velocity in the $\theta$ direction, and $U_\varphi$ is the velocity in the $\varphi$ direction.

The temperature fields, the solute field, the liquid composition at the interface, and the moving velocity of the interface affected by the far-field flow can be expressed as

$$\{T_{\rm L}, T_{\rm S}, C, C_{\rm I}, v\} \sim q_0 + q_1 U_\infty + {\rm O}\left(U_\infty^2\right), \tag{11}$$

where $q_0$ represents the part unaffected by the far-field flow, $T_{\rm L0}$ and $T_{\rm S0}$ are the liquid and the solid temperature fields without the flow, respectively, $C_0$ is the liquid solute field without the flow. Here $T_{\rm L0}$, $T_{\rm S0}$, and $C_0$ satisfy the Laplace equation

$$\Delta T_{\rm L0} = 0, \tag{12}$$

$$\Delta T_{\rm S0} = 0, \tag{13}$$

$$\Delta C_0 = 0. \tag{14}$$

Combining with Eqs. (5)–(7), we obtain the solutions of $T_{\rm L0}$, $T_{\rm S0}$, $C_0$ as

$$\begin{aligned} T_{\rm L0} &= v_0 h_\Delta R_0^2/(k_{\rm L} r) + T_{\rm M} + m_{\rm L} C_{\rm I0} \\ &\quad - 2\Gamma T_{\rm M}/R_0 - v_0 h_\Delta R_0/k_{\rm L}, \end{aligned} \tag{15}$$

$$T_{\rm S0} = T_{\rm M} + m_{\rm L} C_{\rm I0} - 2\Gamma T_{\rm M}/R_0, \tag{16}$$

$$\begin{aligned} C_0 &= v_0 C_{\rm I0}\left(1-k_0\right) R_0^2/(Dr) + C_{\rm I0} \\ &\quad - v_0 C_{\rm I0}\left(1-k_0\right) R_0/D, \end{aligned} \tag{17}$$

where $C_{\rm I0}$ and $v_0$ represent the liquid composition at the interface and the moving velocity of the interface without the flow, respectively. Their values can be obtained from far-field composition $C_\infty$ and far-field undercooling $\Delta T_\infty = T_{\rm M} + m_{\rm L} C_0 - T_\infty$,

$$C_{\rm I0} = \left(-A_1 - \sqrt{A_1^2 - 4 m_{\rm L} A_2}\right)/(2 m_{\rm L}), \tag{18}$$

$$v_0 = D\left(1 - C_\infty/C_{\rm I0}\right)/[\left(1-k_0\right) R_0], \tag{19}$$

$$\begin{aligned} A_1 &= \frac{-2\Gamma T_{\rm M}}{R_0} - \frac{D h_\Delta}{k_{\rm L}\left(1-k_0\right)} + \Delta T_\infty \\ &\quad - m_{\rm L} C_\infty, \end{aligned} \tag{20}$$

$$A_2 = D h_\Delta C_\infty/[k_{\rm L}\left(1-k_0\right)]. \tag{21}$$

Then inserting Eq. (11) into Eqs. (2)–(4), we obtain

$$\begin{aligned} &\boldsymbol{U}\cdot\boldsymbol{\nabla}\left(\sum_{j=0}^{+\infty} U_\infty^j T_{{\rm L}j}\right) \\ &= \left(k_{\rm L}/C_{\rm pL}\right)\Delta\left(\sum_{j=0}^{+\infty} U_\infty^j T_{{\rm L}j}\right), \end{aligned} \tag{22}$$

$$\Delta\left(\sum_{j=0}^{+\infty} U_\infty^j T_{{\rm S}j}\right) = 0, \tag{23}$$

$$\boldsymbol{U}\cdot\boldsymbol{\nabla}\left(\sum_{j=0}^{+\infty} U_\infty^j C_j\right) = D\Delta\left(\sum_{j=0}^{+\infty} U_\infty^j C_j\right), \tag{24}$$

where $T_{{\rm L}j}$, $T_{{\rm S}j}$ and $C_j$ represent the perturbation series of the temperature fields and the solute field, respectively, $U_\infty$ is the far-field velocity, and $j$ represents the order of $U_\infty$.

Substituting $\boldsymbol{U}$ with Eqs. (8)–(10) yields

$$\begin{aligned} &\frac{U_R}{U_\infty}\cdot\frac{\partial T_{{\rm L},j-1}}{\partial r} + \frac{U_\theta}{U_\infty}\frac{1}{r}\frac{\partial T_{{\rm L},j-1}}{\partial\theta} \\ &= \left(k_{\rm L}/C_{\rm pL}\right)\Delta T_{{\rm L}j}, \end{aligned} \tag{25}$$

$$\Delta T_{{\rm S}j} = 0, \tag{26}$$

$$\frac{U_R}{U_\infty}\cdot\frac{\partial C_{j-1}}{\partial r} + \frac{U_\theta}{U_\infty}\frac{1}{r}\frac{\partial C_{j-1}}{\partial\theta} = D\Delta C_j. \tag{27}$$

Set $j = 1$ in Eqs. (25)–(27), we can obtain the solutions of $T_{\rm L1}$, $T_{\rm S1}$, and $C_1$ as

$$\begin{aligned} T_{\rm L1} &= \left(\frac{1}{2} - \frac{3}{4}\frac{R_0}{r} + a_1\frac{R_0^2}{r^2} - \frac{1}{8}\frac{R_0^3}{r^3}\right) \\ &\quad \times \cos\theta A_{T_{\rm L1}} C_{\rm pL}/k_{\rm L}, \end{aligned} \tag{28}$$

$$T_{\rm S1} = \cos\theta \frac{A_{T_{\rm L1}} C_{\rm pL}}{k_{\rm L}} \left(a_1 - \frac{3}{8}\right) \frac{r}{R_0}, \quad (29)$$

$$C_1 = \cos\theta \frac{A_{C_1}}{D} \left(\frac{1}{2} - \frac{3}{4}\frac{R_0}{r} + a_2 \frac{R_0^2}{r^2} - \frac{1}{8}\frac{R_0^3}{r^3}\right), \quad (30)$$

where

$$A_{T_{\rm L1}} = v_0 h_\Delta R_0^2 / k_{\rm L}, \quad (31)$$

$$A_{C_1} = v_0 C_{\rm I0} (1 - k_0) R_0^2 / D. \quad (32)$$

There are two undetermined parameters, $a_1$ and $a_2$, in Eqs. (28)–(30). Their values can be obtained by using Eqs. (5)–(7). Combining Eqs. (6) and (7), we can obtain the relationship between the temperature and the solute gradients at the solid–liqid interface

$$h_\Delta D \left(\frac{\partial C}{\partial r}\right)_{\rm I} = C_{\rm I} (1 - k_0) \left[k_{\rm L} \left(\frac{\partial T_{\rm L}}{\partial r}\right)_{\rm I} - k_{\rm S} \left(\frac{\partial T_{\rm S}}{\partial r}\right)_{\rm I}\right]. \quad (33)$$

Insert Eqs. (28)–(30) into Eq. (33), we can obtain the relationship between $a_1$ and $a_2$

$$\begin{aligned} &\left[(1 - k_0) v_0 - 2D R_0^{-1}\right] a_2 \\ &+ D^2 \frac{C_{\rm pL}}{k_{\rm L}^2} \left(2k_{\rm L} R_0^{-1} + k_{\rm S} R_0^{-1}\right) a_1 \\ &= D^2 \frac{C_{\rm pL}}{k_{\rm L}^2} \left(\frac{9}{8} k_{\rm L} R_0^{-1} + \frac{3}{8} k_{\rm S} R_0^{-1}\right) \\ &+ \frac{3}{8} (1 - k_{\rm B}) v_0 - \frac{9}{8} D R_0^{-1}. \end{aligned} \quad (34)$$

Insert Eqs. (28)–(30) into Eq. (5), we can obtain the other relationship between $a_1$ and $a_2$

$$\frac{A_{T_{\rm L1}} C_{\rm pL}}{k_{\rm L}} \left(a_1 - \frac{3}{8}\right) = m_{\rm L} \frac{A_{C_1}}{k_{\rm C}} \left(a_2 - \frac{3}{8}\right). \quad (35)$$

Combining Eqs. (34) and (35), we can solve the values of $a_1$ and $a_2$,

$$a_1 = \frac{a_5 a_7 + a_3 a_8}{a_3 a_6 + a_4 a_7}, \quad (36)$$

$$a_2 = \frac{a_5 a_6 - a_4 a_8}{a_3 a_6 + a_4 a_7}, \quad (37)$$

where

$$a_3 = (1 - k_0) v_0 - 2D R_0^{-1}, \quad (38)$$

$$a_4 = C_{\rm pL} (D/k_{\rm L})^2 \left(2k_{\rm L} R_0^{-1} + k_{\rm S} R_0^{-1}\right), \quad (39)$$

$$a_5 = C_{\rm pL} \left(\frac{D}{k_{\rm L}}\right)^2 \left(\frac{9}{8} k_{\rm L} R_0^{-1} + \frac{3}{8} k_{\rm S} R_0^{-1}\right) + \frac{3}{8} (1 - k_0) v_0 - \frac{9}{8} D R_0^{-1}, \quad (40)$$

$$a_6 = A_{T_{\rm L1}} C_{\rm pL} / k_{\rm L}, \quad (41)$$

$$a_7 = m_{\rm L} A_{C_1} / D, \quad (42)$$

$$a_8 = \frac{3}{8} \frac{A_{T_{\rm L1}} C_{\rm pL}}{k_{\rm L}} - \frac{3}{8} m_{\rm L} \frac{A_{C_1}}{D}. \quad (43)$$

Now, the temperature and the solute field under the far-field flow can be expressed as

$$\begin{aligned} T_{\rm L} = {} & v_0 h_\Delta R_0^2 / (k_{\rm L} r) + T_{\rm M} + m_{\rm L} C_{\rm I0} \\ & - v_0 h_\Delta R_0 / k_{\rm L} - \frac{2\Gamma T_{\rm M}}{R_0} + U_\infty \cos\theta \frac{A_{T_{\rm L1}} C_{\rm pL}}{k_{\rm L}} \\ & \times \left(\frac{1}{2} - \frac{3}{4}\frac{R_0}{r} + a_1 \frac{R_0^2}{r^2} - \frac{1}{8}\frac{R_0^3}{r^3}\right) \\ & + {\rm O}\left(U_\infty^2\right), \end{aligned} \quad (44)$$

$$\begin{aligned} T_{\rm S} = {} & T_{\rm M} + m_{\rm L} C_{\rm I0} - 2\Gamma T_{\rm M} / R_0 \\ & + U_\infty \cos\theta \frac{A_{T_{\rm L1}} C_{\rm pL}}{k_{\rm L}} \left(a_1 - \frac{3}{8}\right) \frac{r}{R_0} \\ & + {\rm O}\left(U_\infty^2\right), \end{aligned} \quad (45)$$

$$\begin{aligned} C = {} & \frac{v_0 C_{\rm I0} (1 - k_0) R_0^2}{Dr} - \frac{v_0 C_{\rm I0} (1 - k_0) R_0}{D} + C_{\rm I0} \\ & + U_\infty \cos\theta \frac{A_{C_1}}{D} \left(\frac{1}{2} - \frac{3}{4}\frac{R_0}{r} + a_2 \frac{R_0^2}{r^2} - \frac{1}{8}\frac{R_0^3}{r^3}\right) \\ & + {\rm O}\left(U_\infty^2\right). \end{aligned} \quad (46)$$

Equations (44)–(46) are the solutions of the temperature and the solute fields under the far-field flow. Chen's work[9] only considered the temperature field. For $a_1 = 3/8$, our solutions of the temperature fields are the same as that in Chen's work.[9]

We can obtain the moving velocity of the interface from Eq. (7) and the interface liquid composition from Eq. (46)

$$\begin{aligned} v = {} & v_0 + U_\infty \cos\theta v_0 R_0^2 / D^2 \left[-\frac{D}{R_0}\left(\frac{9}{8} - 2a_2\right)\right. \\ & \left. - v_0 (1 - k_0) \left(a_2 - \frac{3}{8}\right)\right] + {\rm O}\left(U_\infty^2\right), \end{aligned} \quad (47)$$

$$C_{\rm I} = C_{\rm I0} + U_\infty \cos\theta \frac{A_{C_1}}{D} \left(a_2 - \frac{3}{8}\right). \quad (48)$$

## 3. Stability analysis

Under the perturbation, the interface can be described by

$$r = R(\theta, \varphi, t) = R_0(t) + \delta(t) {\rm Y}_{lm}(\theta, \varphi), \quad (49)$$

where $\delta(t)$ represents the infinitesimal amplitude of the perturbation, $l$ and $m$ are integers that represent the order of the spherical harmonic function. The interface moving velocity $v$ can be expressed as

$$\dot{r} = \dot{R} + \dot{\delta} {\rm Y}_{lm}. \quad (50)$$

After the perturbation, we can obtain the solutions of the temperature and the solute fields for the distorted interface from Eqs. (2)–(4)

$$T_{\rm L} = T_{\rm L0} + T_{\rm L1} U_\infty + \delta A_{\delta T_{\rm L}} (r/R_0)^{-l-1} {\rm Y}_{lm}, \quad (51)$$

$$T_{\rm S} = T_{\rm S0} + T_{\rm S1}U_\infty + \delta A_{\delta T_{\rm S}} (r/R_0)^l \, {\rm Y}_{lm}, \quad (52)$$

$$C = C_{\rm U0} + C_{\rm U1}U_\infty + \delta A_{\delta C} (r/R_0)^{-l-1} \, {\rm Y}_{lm}, \quad (53)$$

where $l$ represents the order of the instability mode. If $l = 0$, the interface remains spherical. The larger $l$ is, the more complicated the shape of the interface becomes after the perturbation. If $l$ is small, the shape change of the interface is insignificant.

Now the temperature and the solute gradients at the interface become

$$\left(\frac{\partial T_{\rm L}}{\partial r}\right)_{r=R+\delta {\rm Y}_{lm}} = \left(\frac{\partial T_{\rm L}}{\partial r}\right)_{r=R_0} + \left(\frac{\partial^2 T_{\rm L}}{\partial r^2}\right)_{r=R_0} \delta {\rm Y}_{lm}, \quad (54)$$

$$\left(\frac{\partial T_{\rm S}}{\partial r}\right)_{r=R+\delta {\rm Y}_{lm}} = \left(\frac{\partial T_{\rm S}}{\partial r}\right)_{r=R_0} + \left(\frac{\partial^2 T_{\rm S}}{\partial r^2}\right)_{r=R_0} \delta {\rm Y}_{lm}, \quad (55)$$

$$\left(\frac{\partial C}{\partial r}\right)_{r=R+\delta {\rm Y}_{lm}} = \left(\frac{\partial C}{\partial r}\right)_{r=R_0} + \left(\frac{\partial^2 C}{\partial r^2}\right)_{r=R_0} \delta {\rm Y}_{lm}. \quad (56)$$

The temperature and the liquid composition at the interface become

$$(T_{\rm L})_{r=R+\delta {\rm Y}_{lm}} = (T_{\rm L})_{r=R_0} + \left(\frac{\partial T_{\rm L}}{\partial r}\right)_{r=R_0} \delta {\rm Y}_{lm} = (T_{\rm S})_{r=R_0} + \left(\frac{\partial T_{\rm S}}{\partial r}\right)_{r=R_0} \delta {\rm Y}_{lm}, \quad (57)$$

$$(C)_{r=R+\delta {\rm Y}_{lm}} = (C)_{r=R_0} + \left(\frac{\partial C}{\partial r}\right)_{r=R_0} \delta {\rm Y}_{lm}. \quad (58)$$

According to the Gibbs–Thomson equation (Eq. (5)), we obtain

$$(T_{\rm L})_{r=R+\delta {\rm Y}_{lm}} = T_{\rm M} + m_{\rm L} (C)_{r=R+\delta {\rm Y}_{lm}} - 2\Gamma T_{\rm M}/R_0 - \Gamma T_{\rm M} (l-1)(l+2) \delta {\rm Y}_{lm}/R_0^2. \quad (59)$$

Substitute Eqs. (58) and (59) into Eq. (57), we obtain

$$A_{\delta T_{\rm L}} = m_{\rm L} \left[A_{\delta C} + \left(\frac{\partial C}{\partial r}\right)_{r=R_0}\right] - \left(\frac{\partial T_{\rm L}}{\partial r}\right)_{r=R_0} + \Gamma T_{\rm M} (l-1)(l+2)/R_0^2, \quad (60)$$

$$A_{\delta T_{\rm S}} = m_{\rm L} \left[A_{\delta C} + \left(\frac{\partial C}{\partial r}\right)_{r=R_0}\right] - \left(\frac{\partial T_{\rm S}}{\partial r}\right)_{r=R_0} + \Gamma T_{\rm M} (l-1)(l+2)/R_0^2. \quad (61)$$

Substitute Eqs. (54)–(56) into Eqs. (6) and (7), we can obtain the growth rate of the interface perturbation amplitude $S = \dot{\delta}/\delta$ as

$$S = \frac{\dfrac{B_1 R_0}{k_{\rm L}(-l-1) - k_{\rm S} l} - \dfrac{m_{\rm L} B_2 R_0}{D(-l-1) + v R_0 (1-k_0)} + \dfrac{\Gamma T_{\rm M} (l-1)(l+2)}{R_0^2}}{\dfrac{h_\Delta}{(-k_{\rm L} l - k_{\rm L} - k_{\rm S} l)/R_0} - \dfrac{C_{\rm I0}(1-k_0) m_{\rm L}}{D(-l-1)/R_0 + v(1-k_0)}}, \quad (62)$$

where

$$B_1 = v_0 h_\Delta (l-1)/R_0 + U_\infty A_{T_{\rm L1}} C_{\rm pL} \cos\theta / R_0^2 \times \left[(-l-1)\left(\frac{9}{8} - 2a_1\right) - l\frac{k_{\rm S}}{k_{\rm L}}\left(a_1 - \frac{3}{8}\right) - (6a_1 - 3)\right], \quad (63)$$

$$B_2 = v_0 C_{\rm I0} (l-1)(1-k_0)/R_0 + U_\infty A_{C_1} \cos\theta / R_0^2 \times \left[(-l-1)\left(\frac{9}{8} - 2a_1\right) - (6a_1 - 3)\right]. \quad (64)$$

If we set $U_\infty = 0$, then we can obtain the growth rate of the interface perturbation amplitude without the flow

$$S_0 = \frac{k_{\rm L}(l-1)}{R_0 h_\Delta}\left\{ - G_{\rm L} - \frac{T_{\rm M}\Gamma}{R_0^2} \times \frac{L\chi[2p(1-k_0) - (l+1)]}{l+1+lk_{\rm S}/k_{\rm L} + \chi 2p(1-k_0) - \chi(l+1)}\right\}, \quad (65)$$

where

$$G_{\rm L} = -v_0 h_\Delta / k_{\rm L}, \quad (66)$$

$$L = (l+1)(l+2) + l(l+2) k_{\rm S}/k_{\rm L}, \quad (67)$$

$$\chi = h_\Delta D/[k_{\rm L} m_{\rm L} C_{\rm I0} (1-k_0)], \quad (68)$$

$$p = v_0 R_0/(2D). \quad (69)$$

It can be seen that the growth rate of the interface perturbation amplitude is consistent with Trivedi's criterion[14] for $U_\infty = 0$. This means that our criterion is the same as Trivedi's when there is no flow. Our work extends Trivedi's criterion into the case of far-field flow.

The stability of the interface with respect to a perturbation depends on the sign of Eq. (62). If $S > 0$ for any $l$, then the perturbation amplitude grows with time and this means that the spherical interface will become unstable. If $S < 0$ for all $l$, then all perturbation amplitudes will decay with time, which means that the spherical interface will remain stable.

The first term of the denominator of Eq. (62) is obviously negative. According to Eq. (47), $D(-l-1)/R_0 + v(1-k_0) = (D/R_0)[-l - C_\infty/C_{\rm I0}] + {\rm O}(U_\infty) < 0$. This means that the second term of the denominator of Eq. (62) is also negative. Now the sign of $S$ depends on the sign of the numerator of Eq. (62). If the numerator is negative, $S > 0$. If $l$ is infinitely large, the numerator of $S$ will tend to be $\Gamma T_{\rm M} l^2/R_0^2 > 0$, obviously $S < 0$. This means that the interface energy provides the high frequency stability for the interface. When the order of the interface perturbation is $l = 0$ or 1, the change of the interface is insignificant, the interface remains spherical. When $l = 2$, the spherical interface turns into an elliptical one. So $l = 2$ is the lowest order with which we can observe the shape change of the interface. When $l = 2$, the numerator of $S$ turns into

$$S_{\rm nm} = \frac{-G_{\rm L}}{-3 - 2k_{\rm S}/k_{\rm L}} + \frac{m_{\rm L} G_{\rm C}}{-2 - C_\infty/C_{\rm I0}} + \frac{4\Gamma T_{\rm M}}{R_0^2} + {\rm O}(U_\infty), \quad (70)$$

where $G_{\rm C}$ is the solute gradient of the melt. If we can assume $k_{\rm S}/k_{\rm L} \approx 1$, the value of $C_\infty/C_{\rm I0}$ is small and can be neglected. We set $U_\infty = 0$, then equation (70) will turn into

$$S_{\rm nm} \approx -\frac{1}{2}\left(-\frac{2G_{\rm L}}{5} + m_{\rm L} G_{\rm C}\right) + \frac{4\Gamma T_{\rm M}}{R_0^2}. \quad (71)$$

Now we can obtain the following stability criterion for $l = 2$:

$$-\frac{2G_{\rm L}}{5} + m_{\rm L} G_{\rm C} - \frac{8\Gamma T_{\rm M}}{R_0^2} < 0, \quad \text{(stable)}, \quad (72)$$

$$-\frac{2G_{\rm L}}{5} + m_{\rm L} G_{\rm C} - \frac{8\Gamma T_{\rm M}}{R_0^2} > 0, \quad \text{(unstable)}. \quad (73)$$

The stability criterion of the MS theory[18] is

$$-\frac{1}{2}(G_{\rm L} + G_{\rm S}) + m_{\rm L} G_{\rm C} < 0, \quad \text{(stable)}, \quad (74)$$

$$-\frac{1}{2}(G_{\rm L} + G_{\rm S}) + m_{\rm L} G_{\rm C} < 0, \quad \text{(unstable)}. \quad (75)$$

We can see the similarity between the two stability criteria. The difference is caused by the change from a planar interface to the spherical interface. When $l > 2$, the shape change of the interface is more insignificant, the stabilizing effect of $\Gamma$ will be enhanced. Therefore when $l$ is large enough, the interface is always stable due to the stabilizing effect of surface energy $\Gamma$.

The correction of the far-field flow to the liquid temperature field is $T_{\rm L1}$, which satisfies

$$\frac{\boldsymbol{U}}{U_\infty} \cdot \boldsymbol{\nabla} T_{\rm L0} = \frac{k_{\rm L}}{C_{\rm pL}} \Delta T_{\rm L1}. \quad (76)$$

In the up-wind direction, $\cos\theta < 0$, $U_R < 0$, and $\partial T_{\rm L0}/\partial r < 0$, this means that the right-hand side of Eq. (76) is positive. Combining the condition of $\partial T_{\rm L1}/\partial r\big|_{r\to+\infty} = 0$, we have

$$\int_{R_0}^{+\infty} r^2 \Delta T_{\rm L1}\,{\rm d}r \approx \int_{R_0}^{+\infty} \frac{\partial}{\partial r}\left(r^2 \frac{\partial T_{\rm L1}}{\partial r}\right){\rm d}r = -R_0^2 \left.\frac{\partial T_{\rm L1}}{\partial r}\right|_{r=R_0} > 0. \quad (77)$$

This means that the correction of the far-field flow to the temperature gradient at the interface with $\cos\theta < 0$ is negative, which means that the absolute value of the temperature gradient at the interface with $\cos\theta < 0$ is larger than that without the flow.

The correction of the far-field flow to the solute field is $C_{\rm U1}$, which satisfies

$$\frac{\boldsymbol{U}}{U_\infty} \cdot \boldsymbol{\nabla} C_{\rm U0} = D \Delta C_{\rm U1}. \quad (78)$$

Similarly, we can deduce that the absolute value of the solute gradient at the interface with $\cos\theta < 0$ is larger than that without the flow. The solute and the temperature gradients are both negative. So with the increase of the absolute values of both gradients, the effect of the constitutional supercooling is enhanced in the up-wind direction compared to that without the flow. This means that the interface becomes more unstable under the far-field flow. In the down-wind direction, $\cos\theta > 0$, the effect of the constitutional supercooling is reduced compared to that without the flow. The position with the maximum growth rate of perturbation amplitude at the interface decides the stability of the whole interface. Since $\cos\theta < 0$, the crystal interface is more unstable than that without the flow, this means that the spherical interface becomes unstable under the influence of the far-field flow.

If we consider the relative stability, then the perturbation can grow no faster than the growth of the spherical interface itself, i.e., $S' = S - v/R_0 < 0$. Figure 2 shows the variation of $S'$ with $l$ with an undercooling of 3.0 K and a crystal radius of 30 μm for SCN–1.0 wt.% water alloy. The far-field velocity is

$U_\infty = 1.1 \times 10^{-6}$ m/s. The thermal-physical parameters of the SCN–1.0 wt.% water alloy are listed in Table 1.[19] We can see from Fig. 2 that the growth rate of the perturbation amplitude in the up-wind direction is larger than that in the down-wind direction. The growth rate of the perturbation amplitude gets its maximum value when $\theta = 180°$. When the far-field velocity $U_\infty$ increases, the up-wind side will lose stability sooner than the down-wind side. The fastest growing perturbation decides the shape of the interface after losing the stability. So it is important to study the value of $l$ that has the fastest growing rate. If we assume $S'$ gets its maximum value when $l = l_{\max}$, then $l_{\max}$ decreases from $\theta = 180°$ to $\theta = 0°$.

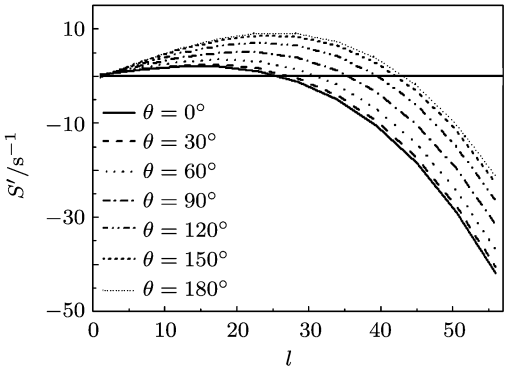



**Fig. 2.** The $S'$ versus $l$ for $R_0 = 30$ μm, $\Delta T_\infty = 3.0$ K, and $U_\infty = 1.1 \times 10^{-6}$ m/s at different positions of the interface.

**Table 1.** Thermal-physical parameters of SCN–water alloy.

| Parameter | Value |
|---|---|
| $k_0$ | 0.001 |
| $D$ | $1.27 \times 10^{-9}$ m$^2$/s |
| $C_\infty$ | 8.0 wt.% |
| $\rho$ | 1016 kg/m$^3$ |
| $k_{\rm L}$ | 0.222 J/(m·s·K) |
| $k_{\rm S}$ | 0.224 J/(m·s·K) |
| $m_{\rm L}$ | −7.16 K/wt.% |
| $h_\Delta$ | $4.57 \times 10^7$ J/m$^3$ |
| $\Gamma$ | $1.959 \times 10^{-10}$ m |
| $T_{\rm M}$ | 331.24 K |
| $C_{\rm pL}$ | $1.9375 \times 10^6$ J/K/m$^3$ |

Figure 3 shows the effect of the crystal radius on $S'$. When $\Delta T_\infty = 0.3$ K, the critical stability radius without the flow is $R_{\rm C}^* = 9$ μm. When $U_\infty = 5 \times 10^{-6}$ m/s, the critical stability radius decreases to 6.15 μm. This further verifies that the far-field flow reduces the relative stability of the interface. When the crystal radius $R_0$ increases, $l_{\max}$ corresponding to the maximum of $S'$ increases too. Comparing to $S'$ at $\theta = 90°$ which represents the growth rate of the perturbation amplitude without the flow, $S'$ in the up-wind direction increases and that in the down-wind direction decreases, which means that the far-field flow makes the up-wind side of the interface more unstable and the down-wind side more stable.

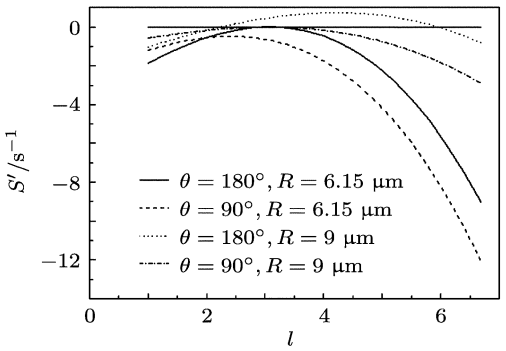



**Fig. 3.** The $S'$ versus $l$ for $\Delta T_\infty = 0.3$ K and $U_\infty = 5 \times 10^{-6}$ m/s with different crystal radii.

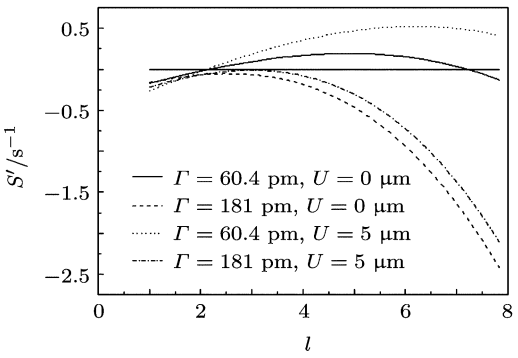



**Fig. 4.** The $S'$ versus $l$ for $\Delta T_\infty = 0.3$ K with different $\Gamma$ and $U_\infty$.

Figure 4 shows the effect of surface energy $\Gamma$ on $S'$. We can see that the growth rate of the perturbation amplitude decreases with the increasing $\Gamma$. The effect of $\Gamma$ is more significant with the high frequency perturbations than that with the low frequency perturbations. This is because $\Gamma$ affects the curvature supercooling that comes from the curvature change of the interface. The curvature change of the interface with a large $l$ is more significant than that with a small value $l$. According to Eq. (59), $\Gamma$ is associated with $(l-1)(l+2)$, this means that the effect of $\Gamma$ is more significant with a larger perturbation frequency $l$. The existence of the far-field flow can enhance the growth rate of the perturbation amplitude compared with that without the flow. It can be seen from Fig. 4

that this enhancing effect is more significant with a small $\Gamma$ and a large $l$. This is because the surface energy provides the stabilizing effect, when $\Gamma$ is small, the stabilizing effect is weakened.

Figure 5 shows the effect of far-field composition $C_\infty$ on $S'$. With the increasing $C_\infty$, the growth rate of the perturbation amplitude increases. When $C_\infty$ becomes larger, the absolute value of the solute gradient at the interface increases, therefore the constitutional supercooling effect at the interface is enhanced. Increasing $C_\infty$ makes the interface become more unstable.

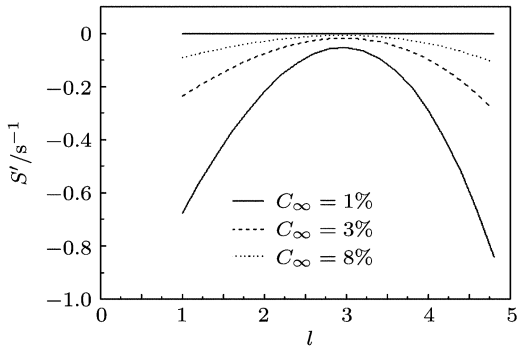



**Fig. 5.** The $S'$ versus $l$ for $\Delta T_\infty = 0.3$ K, $U_\infty = 1.0 \times 10^{-7}$ m/s, and $R_0 = 8.4$ $\mu m$ with different far-field composition $C_\infty$.

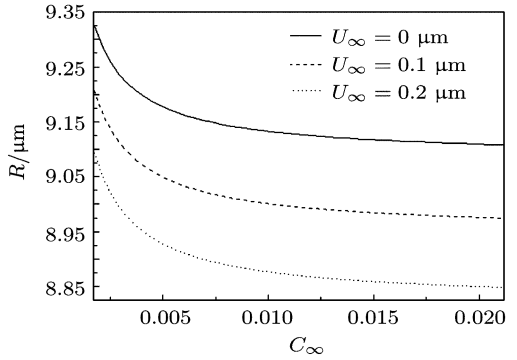



**Fig. 6.** Critical stability radius $R$ versus far-field composition $C_\infty$ with $\Delta T_\infty = 0.3$ K.

Figure 6 shows the variation of the critical stability radius with the far-field composition $C_\infty$ for different $U_\infty$. The critical stability radius decreases with the increasing $C_\infty$. This is due to the enhanced effect of the constitutional supercooling at the interface. The increase of far-field velocity $U_\infty$ also decreases the critical stability radius. In Fig. 6, when $C_\infty = 0.175\%$, the critical stability radii with $U_\infty = 0$ μm/s and $U_\infty = 0.2$ μm/s are 9.32545 μm and 9.09331 μm, respectively, the difference is 0.23214 μm. When $C_\infty = 2.12\%$, the critical stability radii with $U_\infty = 0$ μm/s and $U_\infty = 0.2$ μm/s are 9.10829 μm and 8.84845 μm, respectively, the difference is 0.25984 μm. We can see that the reducing effect of the far-field flow on the critical stability radius slowly increases with the larger far-field composition $C_\infty$. This is because the far-field flow enhances the constitutional supercooling effect at the up-wind side of the interface. With the larger far-field composition $C_\infty$, the constitutional supercooling effect is more significant, therefore the effect of the far-field flow is enhanced.

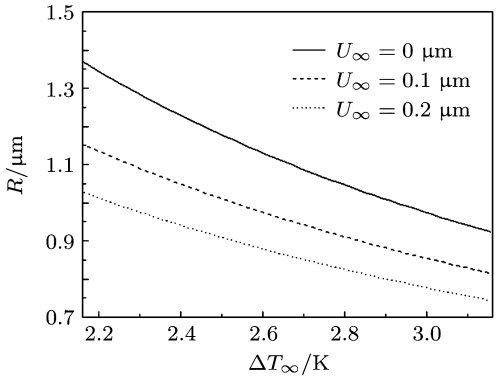



**Fig. 7.** Critical stability radius $R$ versus $\Delta T_\infty$ with different $U_\infty$.

Figure 7 shows the variation of the critical stability radius with the melt undercooling for different $U_\infty$. We can see that the critical stability radius decreases with the increasing melt undercooling no matter whether there is the far-field flow or not. The existence of the far-field flow decreases the critical stability radius.

## 4. Conclusion

With the asymptotic analysis method, we studied the effects of the far-field flow on the temperature and the solute fields around a spherical crystal in a supercooled binary melt. Based on the results, we further obtained the growth rate of the interface perturbation amplitude under the far-field flow. It was found that under the far-field flow, the growth rate of the perturbation amplitude at the up-wind side of the crystal is larger than that at the down-wind side.

As for the order of perturbation $l_{\max}$, which corresponds to the maximum value of the growth rate of the perturbation amplitude, it decreases from $\theta = 180°$ to $\theta = 0°$. Compared to the crystal growth without the flow, the far-field flow enhances the stability of the down-wind side and reduces the stability of the up-wind side. The most unstable point of the interface

is at the top of the up-wind side. The $l_{\max}$ also increases with the increasing crystal radius $R_0$. The far-field flow reduces the stability of the spherical crystal interface. The critical stability radius of the crystal decreases with the increasing far-field velocity $U_\infty$.

The increase of surface energy $\Gamma$ can stabilize the spherical interface. The destabilizing effect of the far-field flow is more significant with a smaller $\Gamma$. The critical stability radius decreases with the increasing $C_\infty$. The reducing effect of the far-field flow on the critical stability radius becomes more significant with the increasing $C_\infty$.

# References


[1] Coriell S R, McFadden G B, Boisvert R F and Sekerka R F 1984 *J. Crystal Growth* **69** 15

[2] Brattkus K and Davis S H 1988 *J. Crystal Growth* **89** 423

[3] Schulze T P and Davis S H 1995 *J. Crystal Growth* **149** 253

[4] Davis S H and Schulze T P 1996 *Metall. Mater. Trans.* A **27** 583

[5] Lin X, Li T, Wang L L, Su Y P and Huang W D 2004 *Acta Phys. Sin.* **53** 3971 (in Chinese)

[6] Zhao D W and Li J F 2007 *Acta Phys. Sin.* **58** 7094 (in Chinese)

[7] Sun D K, Zhu M F, Yang C R, Pan S Y and Dai T 2009 *Acta Phys. Sin.* **58** 285 (in Chinese)

[8] Xing H, Chen C L, Jin K X, Tan X Y and Fan F 2010 *Acta Phys. Sin.* **59** 8218 (in Chinese)

[9] Chen M W, Wang Z D and Xu J J 2007 *Sci. Sin. Tech.* **37** 644

[10] Chen M W, Ni F, Wang Y L, Wang Z D and Xie J X 2011 *Acta Phys. Sin.* **60** 068103 (in Chinese)

[11] Vogel A and Cantor B 1977 *J. Crystal Growth* **37** 309

[12] Li T, Lin X and Huang W D 2006 *Acta Materialia* **54** 4815

[13] Tong L L, Lin X, Zhao L N and Huang W D 2009 *Acta Metallurgica Sinica* **45** 737

[14] Trivedi R 1980 *J. Crystal Growth* **48** 93

[15] Cao B, Lin X, Wang M and Huang W D 2011 *J. Crystal Growth* **327** 140

[16] Cao B, Lin X and Huang W D 2011 *Acta Phys. Sin.* **60** 066403 (in Chinese)

[17] Chen M W, Wang Z D and Sun R J 2007 *Acta Phys. Sin.* **56** 1819 (in Chinese)

[18] Mullins W W and Sekerka R F 1964 *J. Appl. Phys.* **35** 444

[19] Li T, Lin X and Huang W D 2006 *Acta Materialia* **54** 4815